Supplementary figures and table for the article “Citizens' smartphones unravel earthquake shaking in urban areas”

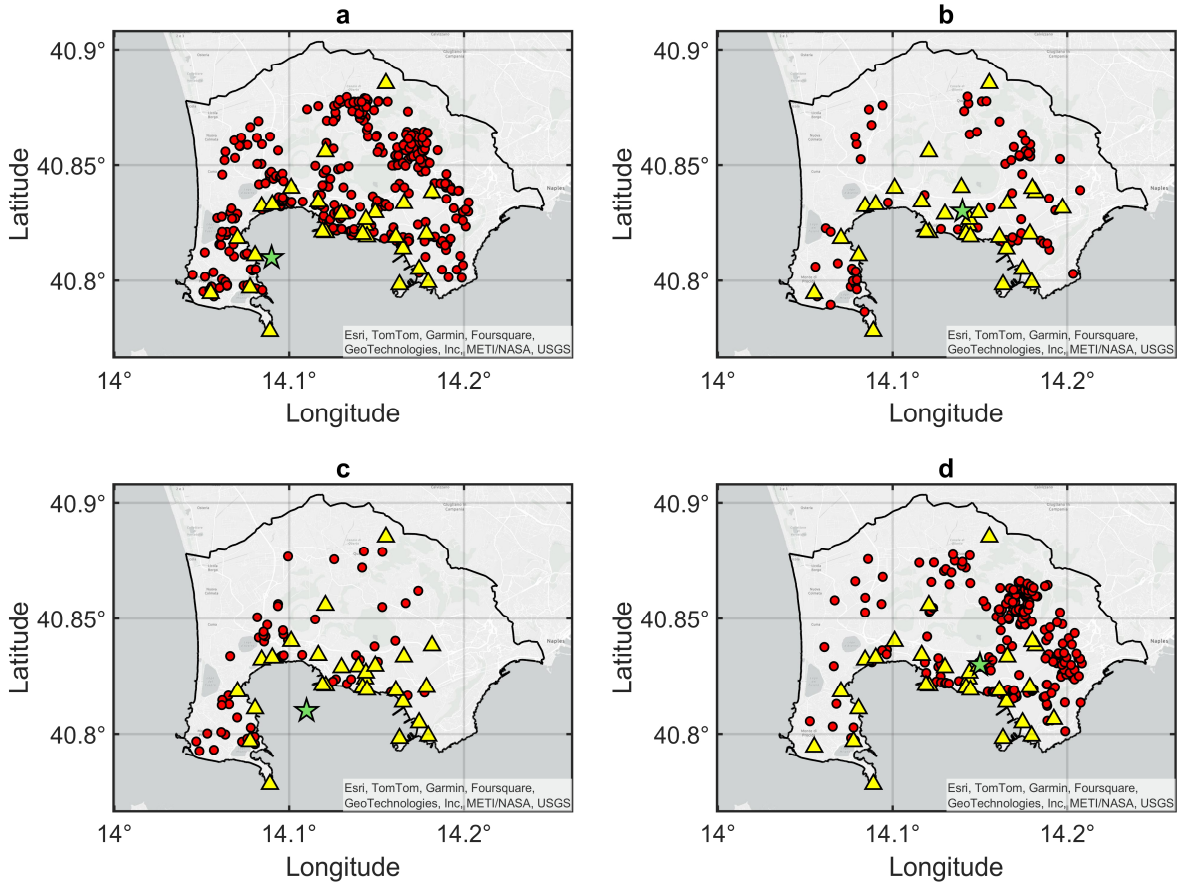

Supplementary Figure 1. Locations of station and smartphone measurements. The figure shows the spatial distribution of the Earthquake Network citizen science initiative smartphones (red circles) and of the seismological stations of the INGV network (yellow triangles) that detected the four earthquakes used to derive the amplification map of Fig. 2. **a**, M3.6, 22 May 2024 06:28:00 event (INGV ID 3838189). **b**, M3.9, 20 May 2024 19:46:14 event (INGV ID 38762031). **c**, M3.9, 27 April 2024 03:44:56 event (INGV ID 38797691). **d**, M4.2, 27 September 2023 01:35:34 (INGV ID 39089101). Green markers are the earthquake epicentres.

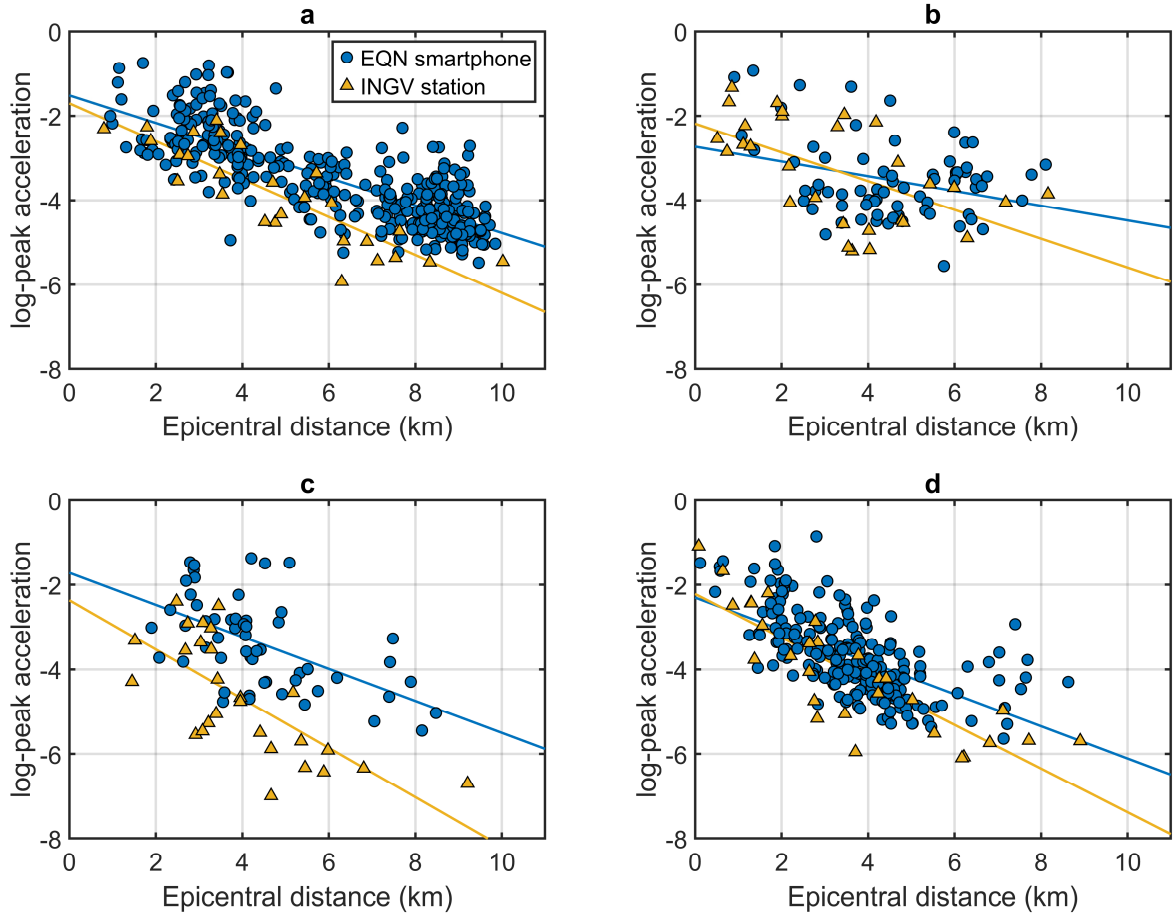

Supplementary Figure 2. Station and smartphone acceleration measurements. Peak accelerations from Earthquake Network citizen science initiative smartphones and INGV network seismological stations used to derive the amplification map. Regression lines describe the fitted decay of the log-peak acceleration considering an isotropic decay model centred on the earthquake epicentre. **a**, M3.6, 22 May 2024 06:28:00 event (INGV ID 3838189). **b**, M3.9, 20 May 2024 19:46:14 event (INGV ID 38762031). **c**, M3.9, 27 April 2024 03:44:56 event (INGV ID 38797691). **d**, M4.2, 27 September 2023 01:35:34 (INGV ID 39089101).

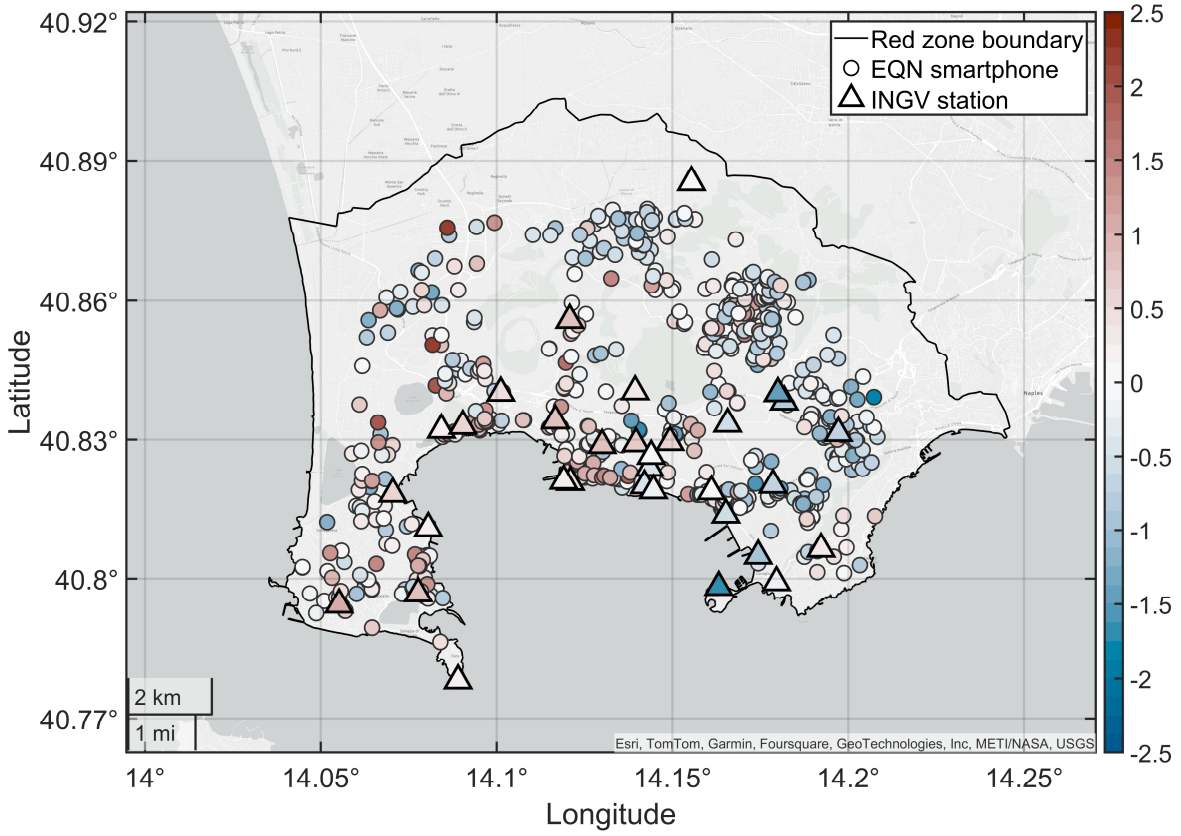

Supplementary Figure 3. Raw log-amplifications. Raw log-amplification are the residuals with respect to the isotropic decays depicted in Extended Data Fig. 2. The figure shows the raw log-amplifications (for the INGV seismological stations and for the smartphones of the Earthquake Network citizen science initiative) obtained for the four events detailed in Extended Data Fig. 1. For INGV stations, the average raw log-amplifications over the four events are shown, while for smartphones the individual raw log-amplifications are shown.

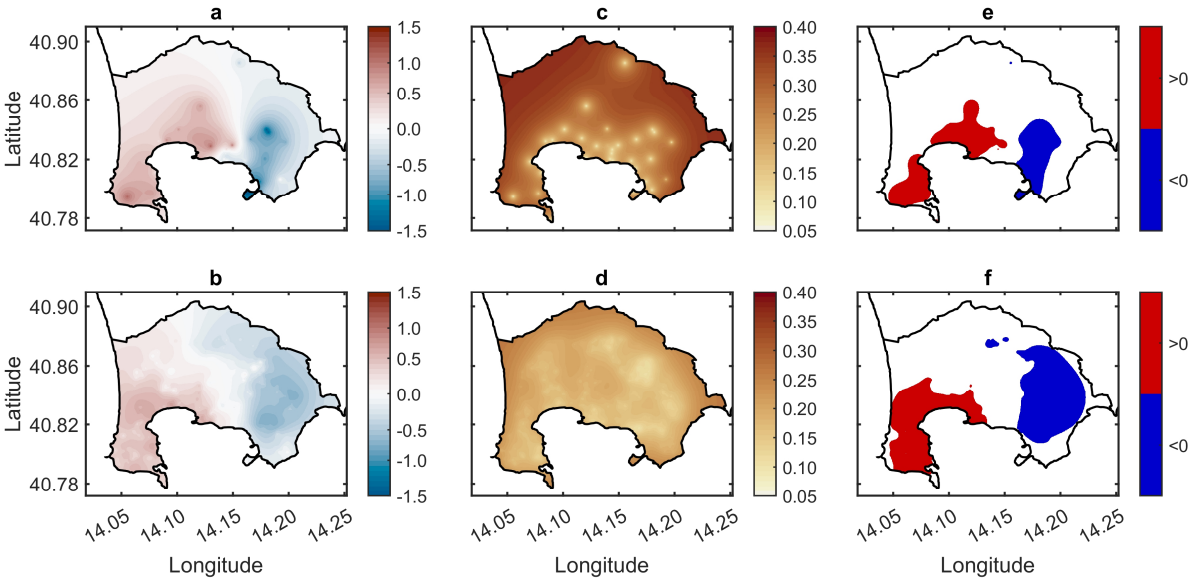

Supplementary Figure 4. Comparison between log-amplification maps. To demonstrate that seismological stations and smartphones similarly capture the spatial pattern of the site amplification, we estimated the log-amplification map considering only station data and only smartphone data. **a**, log-amplification map estimated using station data. **b**, log-amplification map estimated using smartphone data. **c**, standard deviation of the station-data-based log-amplification map. **d**, standard deviation of the smartphone-data-based log-amplification map. **e**, areas where the station-data-based log-amplification map is statistically significantly positive (>0) or negative (<0) considering a 95% confidence interval. **f**, areas where the smartphone-data-based log-amplification map is statistically significantly positive (>0) or negative (<0) considering a 95% confidence interval. The pixel-by-pixel correlation between the log-amplification maps in **a** and **b** is 0.84.

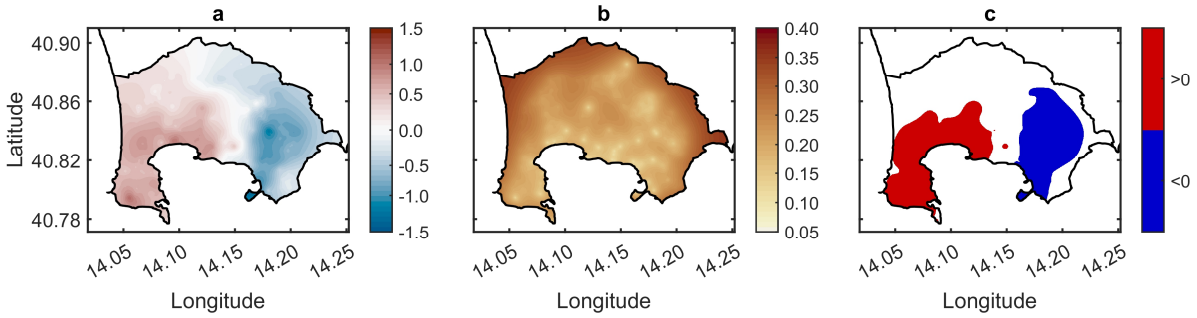

Supplementary Figure 5. Data fusion log-amplification map. a, log-amplification map obtained from the data fusion of station and smartphone data. **b**, standard deviation of the data fusion log-amplification map. **c**, areas where the data fusion log-amplification map is statistically significantly positive (>0) or negative (<0) considering a 95% confidence interval. Thanks to the data fusion, the total area increases from 39.2 km² (30.1% of the red zone area) to 74.9 km² (57.6% of the red zone area) when considering only station data.

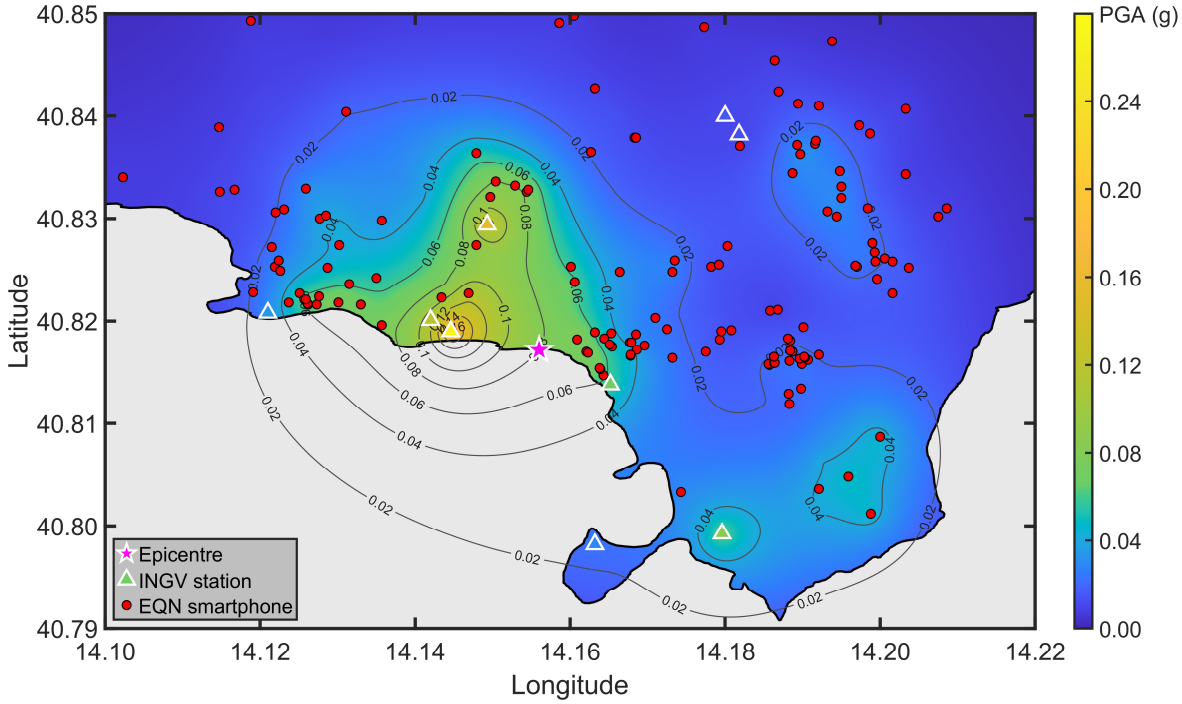

Supplementary Figure 6. Peak ground acceleration ShakeMap lower bound. Our statistical methodology provides the uncertainty of the peak ground acceleration ShakeMap estimated for a given seismic event. To visualize the effect of the uncertainty on the ShakeMap, we fix different probability levels and we show the peak ground acceleration maps with a probability of exceedance equal to these probability levels. The figure shows the peak ground acceleration of 84.4% probability of exceedance for the M4.2 event of 27 September 2023 with an epicentre in the red zone of the Campi Flegrei (INGV ID: 39089101). This is the lower bound for the ShakeMap of Fig 3.

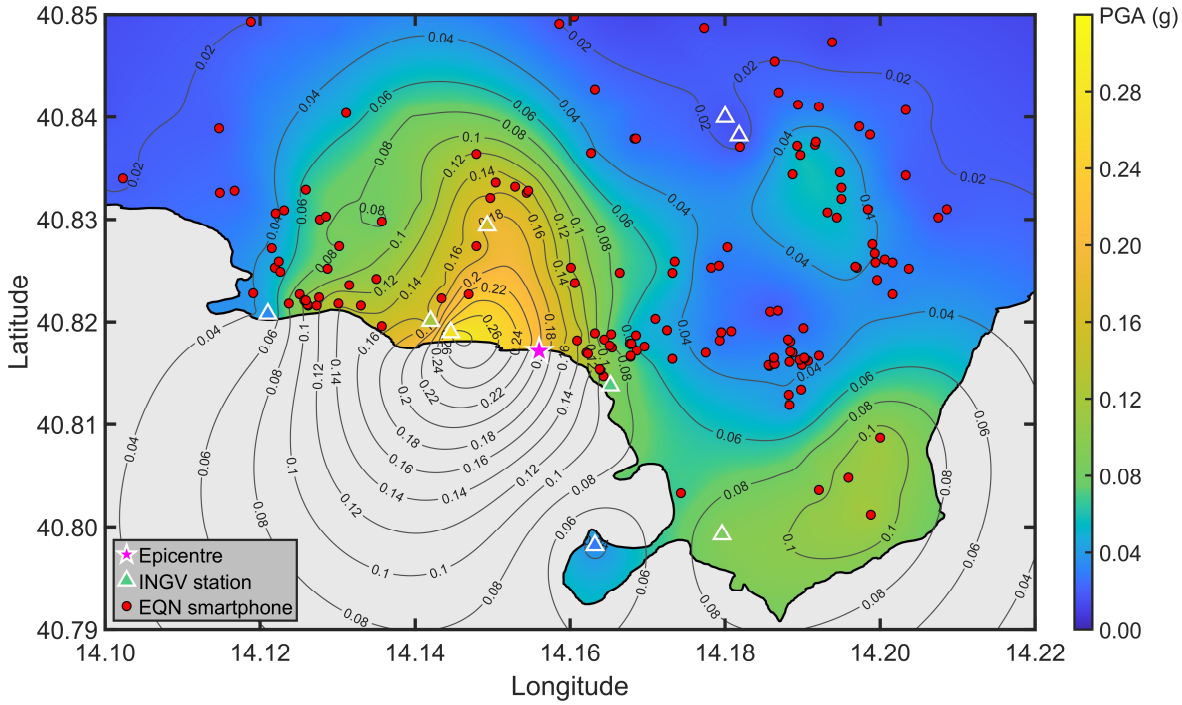

Supplementary Figure 7. Peak ground acceleration ShakeMap upper bound. Peak ground acceleration with a 15.6% exceedance probability for the M4.2 event of 27 September 2023 with an epicentre in the red zone of the Campi Flegrei (INGV event ID: 39089101). This is the upper bound for the ShakeMap of Fig 3.

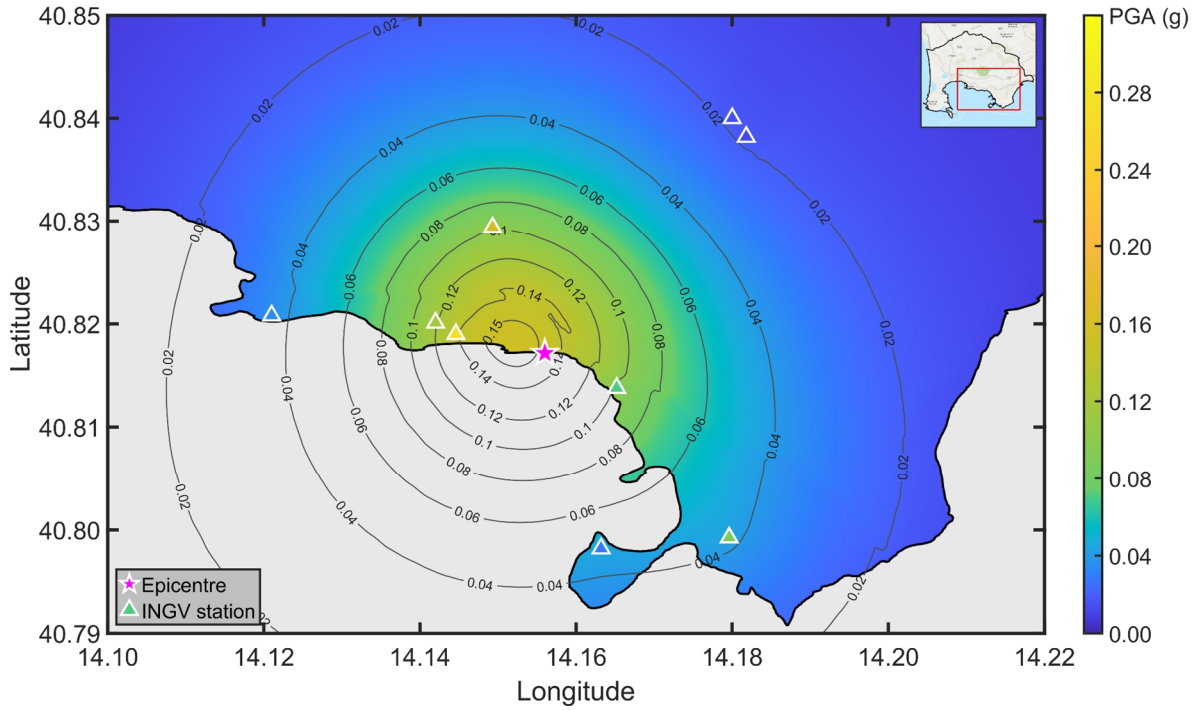

Supplementary Figure 8. INGV peak ground acceleration ShakeMap. Peak ground acceleration ShakeMap estimated by INGV for the M4.2 event on 27 September 2023 (INGV ID: 39089101, data source: https://shakemap.ingv.it/viewLeaflet.html?eventid=36299321). In contrast to the ShakeMap obtained by our approach, the decay of the peak ground acceleration is nearly isotropic and the ShakeMap does not capture local variability at high spatial resolution.

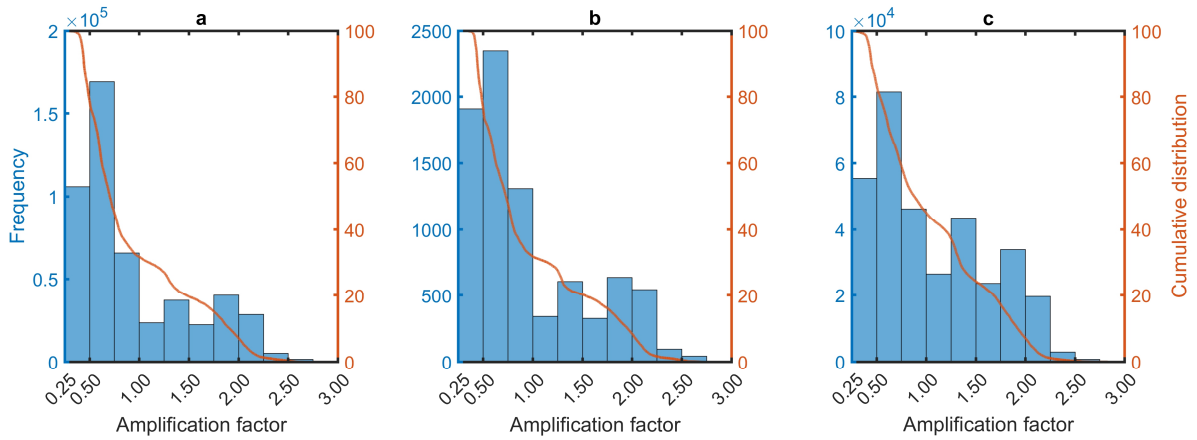

Supplementary Figure 9. Site amplification exposure. a, site amplification exposure for the 498,817 inhabitants of the red zone of Campi Flegrei. **b,** site amplification exposure for the 8,151 Earthquake Network participants in the red zone. **c,** site amplification exposure for the 334,837 buildings in the red zone.

Supplementary Table 1. Estimated model parameters of the statistical data fusion and calibration model described by equation (7) in the Methods section. Considering station and smartphone data, the model is used to derive the site amplification map of Fig. 2. Parameters $\{\beta_{0,PGA,E}, \beta_{1,PGA,E}\}$ and $\{\beta_{0,PSmA,E}, \beta_{1,PSmA,E}\}$ describe the isotropic decay of the peak ground acceleration (in logarithmic scale) recorded by stations and smartphones, respectively. $\boldsymbol{V}_E$ is the variance-covariance matrix of the bivariate Gaussian process used to jointly model stations and smartphone residuals (from the isotropic decay). The Gaussian process has an exponential spatial correlation function with decay parameter θ expressed in metres. Parameters $\phi^2_{PGA,E}$ and $\phi^2_{PSmA,E}$ are the variances of the irreducible model error.

Model parameters	ID: 38381891 Magnitude: 3.6 22 May 2024 06:28:00	ID: 38762031 Magnitude: 3.9 20 May 2024 19:46:14	ID: 38797691 Magnitude: 3.9 27 April 2024 03:44:56	ID: 39089101 Magnitude: 4.2 27 September 2023 01:35:34
$\beta_{0,PGA,E}$	-1.107	-1.106	-1.790	-1.902
$\beta_{1,PGA,E}$	-0.469	-0.493	-0.512	-0.512
$\beta_{0,PSmA,E}$	-1.003	-0.523	-1.753	-1.744
$\beta_{1,PSmA,E}$	-0.381	-0.509	-0.351	-0.393
$\boldsymbol{V}_E$	$\begin{bmatrix} 0.370 & 0.226 \\ 0.226 & 0.167 \end{bmatrix}$	$\begin{bmatrix} 0.864 & 0.802 \\ 0.802 & 0.745 \end{bmatrix}$	$\begin{bmatrix} 0.806 & 0.747 \\ 0.747 & 0.693 \end{bmatrix}$	$\begin{bmatrix} 0.650 & 0.457 \\ 0.457 & 0.321 \end{bmatrix}$
$\theta(m)$	639	7,040	6,226	3,093
$\phi^2_{PGA,E}$	0.046	0.057	0.224	0.101
$\phi^2_{PSmA,E}$	0.222	0.246	0.379	0.349